PHYSICAL REVIEW A **87**, 051603(R) (2013)

Revealing the condensate and noncondensate distributions in the inhomogeneous Bose-Hubbard model

Ushnish Ray and David M. Ceperley
Department of Physics, University of Illinois at Urbana-Champaign, Urbana, Illinois 61801, USA
(Received 6 September 2012; published 13 May 2013)

We calculate the condensate fraction and the condensate and noncondensate spatial and momentum distribution of the Bose-Hubbard model in a trap. From our results, it is evident that using approximate distributions can lead to erroneous experimental estimates of the condensate. Strong interactions cause the condensate to develop pedestal-like structures around the central peak that can be mistaken as noncondensate atoms. Near the transition temperature, the peak itself can include a significant noncondensate component. Using distributions generated from quantum Monte Carlo simulations, experiments can map their measurements for higher accuracy in identifying phase transitions and temperature.

DOI: 10.1103/PhysRevA.87.051603 PACS number(s): 67.85.−d, 03.75.Lm, 05.30.−d, 37.10.Jk

The Bose-Hubbard (BH) model has been the focus of intensive research over the past decade as a prototypical example of strongly correlated physics, especially since the model was realized with cold atoms in optical lattices [1]. Optical lattice experiments (OLE) are prime candidates for quantum simulations due to their extensive tunability and ease of control; they serve as ideal systems to study dynamical phenomena of many-body effects in strongly interacting systems. Before studies can be meaningful, systematic characterization of equilibrium properties is crucial, the most important quantities being temperature (T) and density. However, direct or *in situ* measurements of temperature in OLEs is still unresolved [2,3]. The natural choice for the study of phase transitions is the order parameter, which for the BH model is the condensate fraction $n_0 = N_0/N$, where N_0 is the total number of condensed atoms and N is the number of atoms. Alternatively, the superfluid fraction [4,5] characterizes the transition, but this is not simple to measure in cold atom systems. Accessible observables in experiments include estimates of the entropy and n_0 that come from time-of-flight (TOF) measurements. The former is obtained from TOF measurements of atoms in a harmonic trap (without the lattice), which are then isentropically transferred into the lattice [3,6,7]. The latter could be measured directly from TOF expansions after all fields are "snapped off." n_0 is particularly useful since, combined with entropy, it could be used for thermometry in experiments [2,8].

A major complication in OLEs is the presence of a parabolic confining potential that renders the system inhomogeneous: Multiple domains arranged in concentric shells coexist and, unlike the homogeneous system, n_0 is no longer given by the occupation number at zero momentum. The most common modeling approach to handle the trap is mean-field (MF) theory: e.g., the Hartree-Fock-Bogoliubov-Popov approximation [9–11] for small interaction strengths (U) or the site-decoupled approach for large U [12], together with the local density approximation (LDA). In situations where MF fails or quantitative comparison to measurement is important, we can resort to exact quantum Monte Carlo (QMC) techniques. QMC has been used to directly compare some observables with measurements. However, to the best of our knowledge, the order parameter has not been computed and compared directly to experiment [13].

In the most common approach, experimental TOF images are heuristically fit to obtain the number of condensed atoms under the peaks and the remaining noncondensed atoms. The ratio of the former to the sum of two is defined as the peak weight [8] or the coherence fraction [3] (f_0) that serves as a proxy for n_0. In previous experiments, thermometry was done by comparing full momentum distributions together with f_0, peak width, and the visibility directly to QMC results [8]. The last three observables were further used to characterize the critical temperature (T_c) for the transition from the normal to the superfluid phase. Unfortunately, these probes are not necessarily reliable estimates of the order parameter since the relation between n_0 and f_0 is not well understood [14]. Previous comparisons show large differences [3]. This is unfortunate because n_0 is a simple probe for this transition and is also indicative of the effect of interactions, i.e., the quantum depletion. Combined with the entropy measurements, n_0 would be an excellent probe for the temperature.

The difficulties in characterizing the mapping stems from a poor understanding of the underlying condensate and noncondensate distributions. If they were known, then n_0 could be estimated by counting the number of atoms in the condensate distribution and in the background. (We note that an analytical mean-field theory method has been developed for a homogeneous system [15]. Although qualitatively useful, this method finds limited use in real trapped systems where it must rely on LDA.) Another serious problem is the role of interaction during TOF expansion; some have argued that the effect is small since by the time the wave functions from two adjacent lattice sites start overlapping, the densities would have dropped dramatically [16]. However, others argue that the effects are significant and lead to hydrodynamic effects in TOF images [3]. The crucial quantity that dictates the significance of these effects is the initial density. From two different sets of experimental data, it seems that for low densities (central filling of 1 or less) [8] interaction effects are small, while at large densities [3] (central filling of 3) they could be significant.

In this Rapid Communication, we calculate n_0 and the spatial and momentum distributions for several low-density systems modeled with the BH Hamiltonian:

$$H = -t \sum_{\langle ij \rangle} \hat{a}_i^\dagger \hat{a}_j + \frac{U}{2} \sum_i \hat{n}_i(\hat{n}_i - 1) - \sum_i \tilde{\mu}_i \hat{n}_i, \qquad (1)$$

where t is the hopping integral between nearest-neighbor sites i and j, $\hat{a}_i^\dagger$ ($\hat{a}_i$) is the Boson creation (annihilation) operator, $\hat{n}_i = \hat{a}_i^\dagger \hat{a}_i$ is the number operator, and U is the on-site repulsive interaction. Here, $\tilde{\mu}_i = \mu - V(r_i/a)^2$ includes both the chemical potential term and spherical harmonic confining potential with a, the lattice spacing and $V = \frac{1}{2}m\omega^2$ the curvature that is given by the mass (m) and trap frequency (ω). Energies are given in atomic recoil energy units: $E_r \sim 167$ nK for ^{87}Rb and the laser wavelength $\lambda = 800$ nm that is used to create the lattice. For our simulations, lattices are between 70^3 and 100^3 with open boundary conditions and the number of particles, $N \sim 58\,000$ to $64\,000$.

We calculate the single-particle density matrix $\hat{\rho}_1(i,j) = \langle \hat{a}_i^\dagger \hat{a}_j \rangle$ [4,5,17,18] using the stochastic series expansion and the directed loop update algorithm [19–21]. Then the occupation of the single-particle states is defined by $\hat{\rho}_1|\psi_i\rangle = N_i|\psi_i\rangle$, where the largest eigenvalue N_0 of $\hat{\rho}_1$ gives the number of condensed atoms and $|\psi_0\rangle$ is the condensate wave function. The other atoms $N_{\rm nc} = \sum_{i\neq 0} N_i = N - N_0$ are noncondensed atoms.

For large systems, obtaining all the occupation modes is challenging because of the Monte Carlo noise in $\hat{\rho}_1$ and the complexity of a complete diagonalization of $\hat{\rho}_1$. However, since the condensate is not fragmented and occupies only one mode in these systems, we use an iterative diagonalization procedure to obtain N_0 and the condensate spatial (momentum) wave function $\psi_0(r)$ [$\phi_0(k) = \mathcal{F}[\psi_0(r)]$, where $\mathcal{F}$ is the Fourier transform] [22]. The spatial noncondensate distribution is then given as $n_{\rm nc}(r) = n(r) - N_0|\psi_0(r)|^2$, where $n(r)$ is the spatial density. The total momentum distribution is

$$n(k) = |w(k)|^2 \sum_{jl} e^{ik(j-l)}\rho(j,l) = n_0(k) + \sum_{p=1} n_p(k). \quad (2)$$

$|w(k)|^2$ is the Wannier envelope needed to switch from discrete to continuum space. The last term on the right-hand side is the momentum noncondensate distribution $n_{\rm nc}(k)$. In order to match with experiments we must include finite TOF effects by adding a site dependent phase term to (2) so that $n_p^\tau(k) = |w(k)|^2 N_p \sum_{jl} e^{ik(j-l)-i(m/2\hbar\tau)(j^2-l^2)}\langle j|\psi_p\rangle\langle\psi_p|l\rangle$, where τ is the TOF time, and m is the particle mass [16]. Note $n_0^\tau(k)$ [$n_{\rm nc}^\tau(k)$] is the finite TOF condensate (noncondensate) distribution.

In Figs. 1(a)–1(d), we present the exact $n(r)$ corresponding to large U. [The trap frequency has been adjusted so that

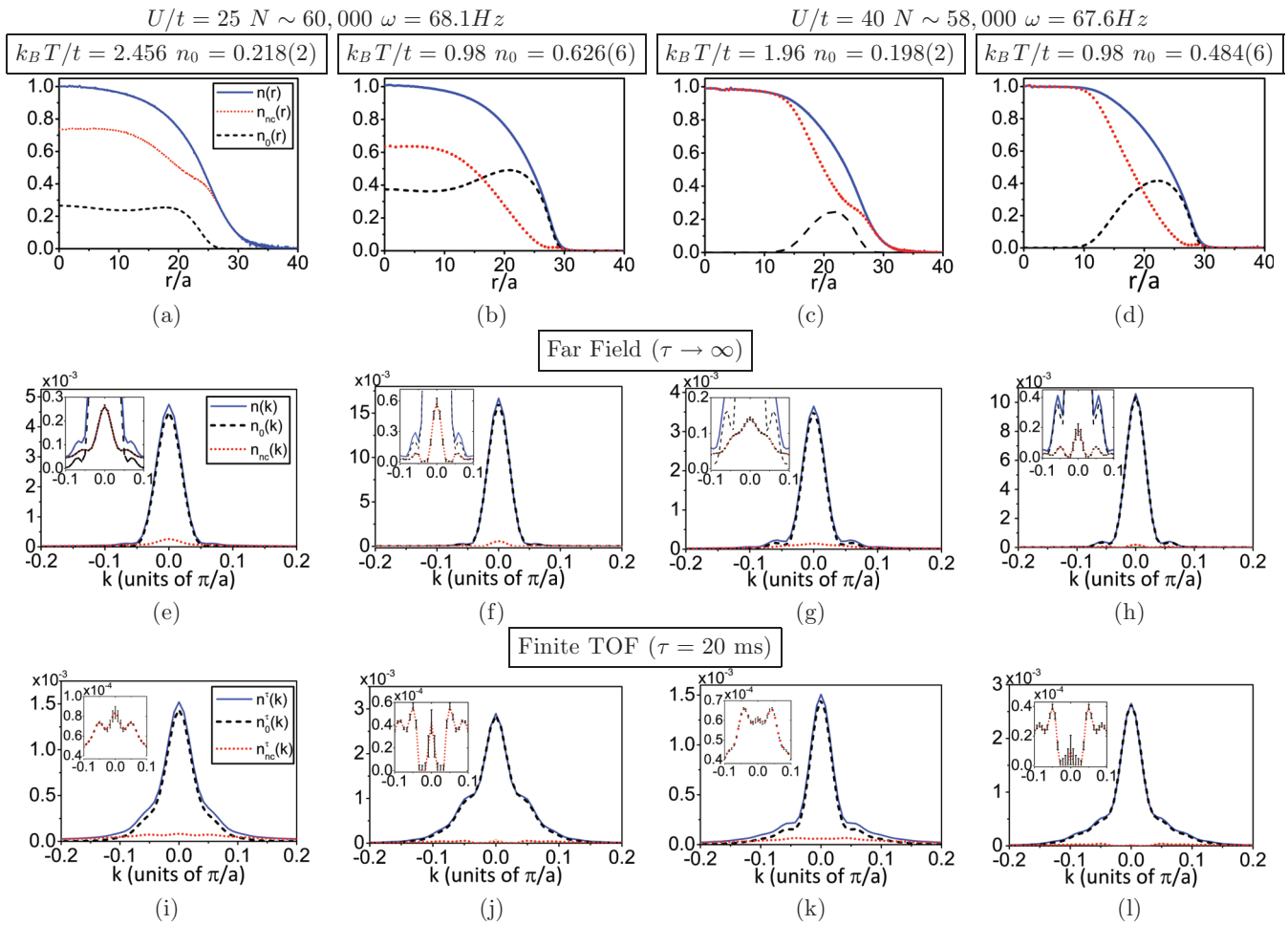

FIG. 1. (Color online) Top row (a)–(d) are the spatial particle densities; middle row (e)–(h) and bottom row (i)–(l) are the column integrated far-field and finite TOF momentum distributions. Insets of (e)–(h) show fine features for all distributions and of (i)–(l) show zoomed versions of the finite TOF noncondensate distribution [$n_{\rm nc}^\tau(k)$]. For the momentum distributions in the middle and bottom row the y axis is in arbitrary units, but the scale is the same for all images.

TABLE I. Statistics of the secondary peaks: fraction of condensate at the maxima of the secondary peak (k_{p2}) and size relative to the central peak.

U/t	k_BT/t	$n_0(k_{p2})/n(k_{p2})$	$n_0(k_{p2})/n(0)$
25	2.46	0.405	0.0098
	0.98	0.742	0.0127
40	1.96	0.696	0.0414
	0.98	0.86	0.034

$n(r=0)=1$; the density is 1 atom/lattice site at the center of the trap.] At $U/t=40$, the Mott insulating (MI) domain appears as an integer plateau. The corresponding column integrated momentum distributions in the far field, shown in Figs. 1(e)–1(h), exhibit secondary peaks similar to [23,24]. Note that these peaks can arise not only due to the finite extent of the condensate but rather all modes [Figs. 1(e)–1(h) insets]. However, it is only around the MI regime that it forms around $k=2\pi/\xi_0$, where ξ_0 is the width of the condensate. This is specifically due to the way the condensate forms between domain boundaries (in this case between the MI and the vacuum). We present statistics of the secondary peak in Table I from which it is evident that its size relative to the central peak and the contribution of the condensate mode to it is much larger (2.8 times at low T and five times at high T) when the system has a MI domain.

Finite TOF effects, presented in Figs. 1(i)–1(l), alter the far-field distributions by suppressing and blurring the central low k values, as expected [16]. Higher order modes of $\hat{\rho}_1$ with rapid spatial variations are not significantly affected by the site dependent phase shift. Thus, the maximum effect is on the condensate distribution. The time scale for the condensate to reach the far field ($\tau_{\rm ff}$) is $\propto R\xi_0(1-\xi_0/2R)$, where R is the radial extent of the condensate. This leads to larger $\tau_{\rm ff}$ for $U/t=25$ and so for the fixed $\tau=20$ ms, the central peak sees a greater suppression (and surrounding region greater enhancement) than $U/t=40$. Although $n(k)$ and $n^\tau(k)$ are both broader due to the secondary peaks, the latter case has relatively more condensate atoms. They would *not* be captured in fitting schemes used in experiments [3,8].

We note that the broader structure is observable within the experimental resolution. Using $\Delta k=(m\lambda\pi/h\tau)\Delta r/a$, where λ is the wavelength of the optical lattice, τ is the expansion time, and Δr is the resolution, we obtain the Δk resolution. Using ^{87}Rb, $\tau=20$ ms, $\lambda=800$ nm, and typical resolving power of $\Delta r=3\,\mu$m gives $\Delta k\sim 0.026\pi/a$. Features in Figs. 1(i)–1(l) are spread over $\Delta k\sim 0.06\pi/a$.

Figures 2(a) and 2(b) show underlying distributions around the transition temperature (T_c) for a weakly (strongly) interacting system with $U/t=3.4$ ($U/t=25$) when $n_{\rm nc}=0.98(5)$ [0.998(6)]. In accordance with previous studies, we see strong central peaks [23,25] even at these warm temperatures. The central and surrounding Bragg peaks contain a significant number of noncondensed atoms. Although the error in estimating n_0 will be specific to the fitting procedure used, we can systematically try to analyze its bounds. We estimate f_0 by calculating the ratio of atoms under the central peak (up to a limit k_l) to the total number of atoms. (The numbers are calculated from column integrated images without the

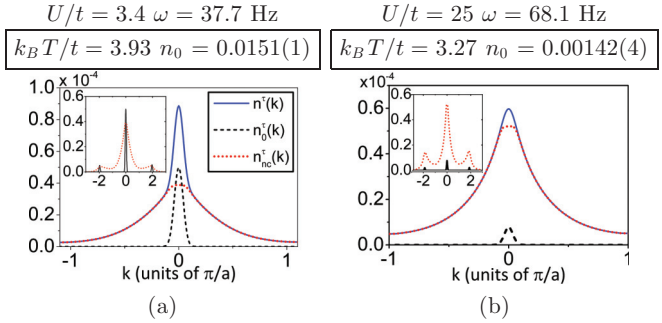

FIG. 2. (Color online) Finite TOF distributions near the transition temperature for a system of $N\sim 64\,000$ atoms with $\tau=20$ ms. Depending on the cut-off k value chosen (k_l) there are 500–5000 atoms for $U/t=3.4$ ($k_l=0.01,0.1$) and 300–1260 atoms for $U/t=25$ ($k_l=0.035,0.075$). The exact numbers are 960 and 90, respectively. The insets show $n_{\rm nc}(k)$ and $n_0(k)$ with three peaks.

Wannier envelope to circumvent the need to deconvolve it.) The range is chosen large enough to accommodate finite optical resolvability in experiments. It should also allow for related fitting procedures.

We present comparisons with exact results in Figs. 3(a) and 3(b) approximated by

$$n_0(T)=n_0^*\left\{1-\exp\left[g\left(1-\frac{T_i}{T}\right)\right]\right\}, \qquad (3)$$

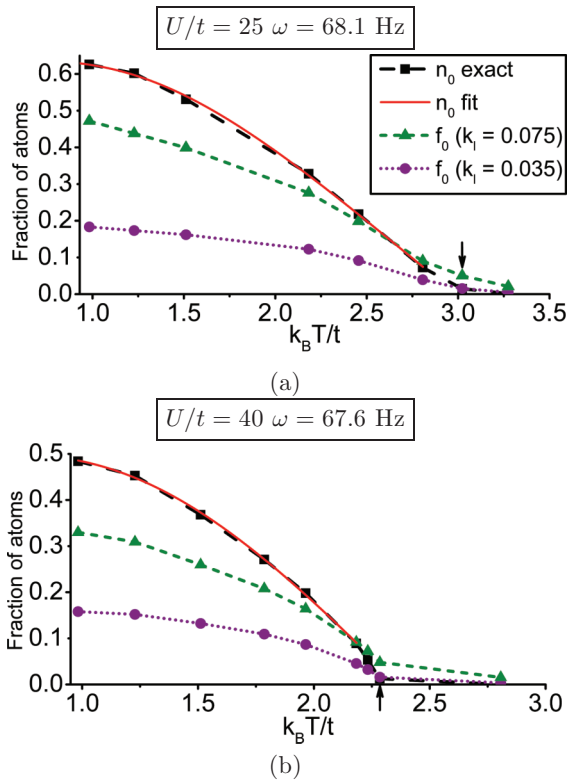

FIG. 3. (Color online) Condensate fraction (n_0) as a function of temperature (T) compared with coherence fraction [$f_0(T)$] measurements for different cutoff k_l [$f_0\equiv\sum_{|k|<k_l}n_0(k)/N$]. We have fit n_0 to (3) where $n_0^*=0.638(7)$ [0.502(6)], $k_BT_i/t=2.99(2)$ [2.36(1)], and $g=1.91(9)$ [2.4(1)] for $U/t=25$ (40). The short arrows indicate $k_BT_c/t=3.023$ (2.285) for $U/t=25$ (40) where $n_0\sim 0.01$. The error bars are smaller than point size used in plots.

away from the critical regime [26]. We see that at low T, the depletion is severely overestimated, whereas around the transition it is underestimated. It is worth noting that general trend of the error is in accordance with f_0 measurements presented in [3], where it is further exacerbated by experimental noise and possible interaction effects during expansion of the gas.

Care is needed in the estimation of T_c using f_0. The specific nature of the error in measuring T_c from $f_0(T)$ will depend on the exact form of the latter. For instance, from our fitting procedure, for $k_l \geqslant 0.035$, $f_0(k_l) > n_0$. If T_c is to be estimated correctly, $|\partial^2 f_0/\partial T^2| > |\partial^2 n_0/\partial T^2|$ is required for rapid convergence to the same $n_0(T) \to 0$. The most rigorous way to estimate T_c would be to study the trap-size scaling behavior analogous to finite size scaling studies done for homogeneous systems that would also identify critical exponents for trapped systems [27]. Here we use a simple working definition $n_0(T_c) \sim 0.01$ that suffices to show that estimates of T_c using f_0 directly would be incorrect: In Figs. 3(a) and 3(b), $k_B T_c/t = 3.022$ (2.284), but using f_0, 3.023 (2.29) $< k_B T_c/t <$ 3.3 (2.81) for $U/t = 25$ (40). Furthermore, a smooth decrease in $f_0(T)$ across the transition may prevent the presence of a clear inflection point thereby making accurate estimates of T_c difficult.

In principle T_c could be estimated from a finite size corrected measurement of f_0 or only $n(k = 0)$, since, as per a theorem due to Chester, Penrose, and Onsager, the latter is expected to be zero (positive) in the absence (presence) of a condensate in the thermodynamic limit for these three-dimensional (3D) systems [14,28]. We point out that alternate schemes have been proposed and used to measure T_c from *in situ* density imaging [29–31], which could be problematic as discussed in [32]. The latter study also suggests measurements from the momentum distributions. However, all these proposals are predicated upon measuring T correctly.

Apart from the mapping technique we consider, alternate ways of measuring T include fitting the tail end of $n(r)$ to a noninteracting model assuming that atoms are normal such as in [30], second-order high-temperature series expansions (HTE2) [33], as well as Fluctuation-Dissipation theorem approaches [34]. Although the first approach might be applicable for weak traps where there is a large tail of (very) low-density normal atoms, it is clearly invalid in the strongly interacting regime in the general case. HTE2 also requires a measurable normal tail where the signal is appreciable. Finally, the last approach could be a feasable alternative despite the requirement of the LDA because in the BH model with the trap there are few shells that are in the critical regime. However, it is not clear whether it will apply to variations of the Bose-Hubbard model, for instance in the presence of disorder. In such cases an effective mapping between the entropy and $n_0(T)$ could be more robust.

We have presented the effects of interactions on the components of the spatial and momentum distributions of bosonic particles in a trapped optical lattice. Our unbiased estimates of $\hat{\rho}_1$ elucidate the potential problems in mapping between the coherence fraction and the exact n_0, and how to account for them. Using exact distributions for QMC, experiments will get more accurate estimates of n_0. In a future work, we will study the effects of interaction during TOF and present comparisons with experimental systems at higher density [35]. We will also explore the entropy (S) mapping using QMC that is needed to compare with $n_0(S)$ from experiments. The method we have presented in this Rapid Communication will be crucial to such studies.

We wish to thank Brian DeMarco, David McKay, Fei Lin, Vito Scarola, Norm Tubman, and Matthias Troyer for useful discussions. This work is supported by the DARPA-OLE program. Computation time was provided by the XSEDE resources at NCSA (University of Illinois in Urbana-Champaign) and TACC (Texas).

[1] M. Greiner, O. Mandel, T. Esslinger, T. Hansch, and I. Bloch, Nature (London) **415**, 39 (2002).

[2] D. McKay, M. White, and B. DeMarco, Phys. Rev. A **79**, 063605 (2009).

[3] D. McKay, Ph.D. thesis, University of Illinois at Urbana-Champaign, 2012.

[4] D. M. Ceperley, Rev. Mod. Phys. **67**, 279 (1995).

[5] A. J. Leggett, *Quantum Liquids: Bose Condensation and Cooper Pairing in Condensed Matter Systems* (Oxford University Press, New York, 2006).

[6] T. Gericke, F. Gerbier, A. Widera, S. F. lling, O. Mandel, and I. Bloch, J. Mod. Opt. **54**, 735 (2007).

[7] M. Pasienski, D. McKay, M. White, and B. DeMarco, Nat. Phys. **6**, 677 (2010).

[8] S. Trotzky, L. Pollet, F. Gerbier, U. Schnorrberger, I. Bloch, N. V. Prokof'ev, B. Svistunov, and M. Troyer, Nat. Phys. **6**, 998 (2010).

[9] A. Rey, K. Burnett, R. Roth, M. Edwards, C. Williams, and C. Clark, J. Phys. B **36**, 825 (2003).

[10] W. Yi, G. D. Lin, and L. M. Duan, Phys. Rev. A **76**, 031602(R) (2007).

[11] J. Anderson, Rev. Mod. Phys. **76**, 599 (2004).

[12] D. van Oosten, P. van der Straten, and H. T. C. Stoof, Phys. Rev. A **63**, 053601 (2001).

[13] A. QMC study using diffusion Monte Carlo was performed in G. E. Astrakharchik and K. V. Krutitsky, Phys. Rev. A **84**, 031604 (2011), for the continuum; however, the results have a trial function bias and are for 100 particles at zero temperature.

[14] Connection between f_0 and n_0 for harmonically confined systems has been explored in W. Mullin, J. Low Temp. Phys. **106**, 615 (1997); Additionally, a basic property connecting $n(k = 0)$ and n_0 is that a zero-momentum occupation $[n(k = 0) > 0]$ is a necessary condition for a BEC in 3D, as shown by J. Carrasquilla and M. Rigol, Phys. Rev. A **86**, 043629 (2012).

[15] D. W. Wang, Phys. Rev. A **80**, 063620 (2009).
[16] F. Gerbier, S. Trotzky, S. Folling, U. Schnorrberger, J. D. Thompson, A. Widera, I. Bloch, L. Pollet, M. Troyer, B. Capogrosso-Sansone, N. V. Prokofev, and B. V. Svistunov, Phys. Rev. Lett. **101**, 155303 (2008).
[17] D. Lewart, V. Pandharipande, and S. Pieper, Phys. Rev. B **37**, 4950 (1988).
[18] O. Penrose and L. Onsager, Phys. Rev. **104**, 576 (1956).
[19] A. W. Sandvik, Phys. Rev. B **59**, R14157 (1999).
[20] A. Dorneich and M. Troyer, Phys. Rev. E **64**, 066701 (2001).
[21] O. F. Syljuasen and A. W. Sandvik, Phys. Rev. E **66**, 046701 (2002).
[22] For a range of systems that we tested, the method is robust and can withstand statistical noise provided we do not enforce Hermitian symmetry; doing so biases the results. For a full discussion refer to U. Ray, F. Lin, J. McMinis, and D. Ceperley (in preparation).
[23] V. A. Kashurnikov, N. V. Prokofev, and B. V. Svistunov, Phys. Rev. A **66**, 031601 (2002).
[24] S. Wessel, F. Alet, M. Troyer, and G. G. Batrouni, Phys. Rev. A **70**, 053615 (2004).
[25] Y. Kato, Q. Zhou, and N. Trivedi, Nat. Phys. **4**, 617 (2008).
[26] We find that the function (3) is a good fit for our QMC data provided $k_bT/t \leqslant 2.183(2.807)$ where $n_0 \geqslant 0.0891(4)[0.0726(3)]$ for $U/t = 25(40)$.
[27] M. Campostrini and E. Vicari, Phys. Rev. Lett. **102**, 240601 (2009).
[28] G. V. Chester, M. E. Fisher, and N. D. Mermin, Phys. Rev. **185**, 760 (1969).
[29] Q. Zhou, Y. Kato, N. Kawashima, and N. Trivedi, Phys. Rev. Lett. **103**, 085701 (2009).
[30] S. Fang, C. M. Chung, P. N. Ma, P. Chen, and D. W. Wang, Phys. Rev. A **83**, 031605(R) (2011).
[31] X. Zhang, C. Hung, S. Tung, and C. Chin, Science **335**, 1070 (2012).
[32] L. Pollet, N. V. Prokofev, and B. V. Svistunov, Phys. Rev. Lett. **104**, 245705 (2010).
[33] P. N. Ma, L. Pollet, and M. Troyer, Phys. Rev. A **82**, 033627 (2010).
[34] Q. Zhou and T. L. Ho, Phys. Rev. Lett. **106**, 225301 (2011).
[35] D. McKay, U. Ray, D. Ceperley, and B. DeMarco (in preparation).